PERGAMON

Engineering Fracture Mechanics 62 (1999) 145–164

Engineering Fracture Mechanics

Plasticity in fretting of coated substrates

Matthew R. Begley[a], John W. Hutchinson[b,*]

[a]*Department of Mechanical Engineering, University of Connecticut, Storrs, CT 06269-3139, USA*
[b]*Division of Engineering and Applied Sciences, Harvard University, Cambridge, MA 02138, USA*

Received 27 July 1998; received in revised form 28 October 1998; accepted 20 December 1998

Abstract

A detailed analysis is performed of the plastic deformation in a metal substrate fretted by a flat-bottomed circular peg under steady normal load and cyclic tangential load. The substrate is coated with a thin layer of soft metal. Two limiting asymptotic problems are identified which characterize small scale yielding behavior in the substrate in the vicinity of the corners of the peg. Deformation within the plastic zone is characterized, including regions of elastic shakedown, steady reversed cyclic plastic straining, and strain ratchetting. Implications for nucleation of fretting cracks are discussed. © 1998 Elsevier Science Ltd. All rights reserved.

Keywords: Fretting; Coated substrates; Plasticity

1. Introduction

Fretting and fretting fatigue are long-standing problems which continue to require attention in a variety of important applications [1,2]. The mechanics for coping with fretting is based almost entirely on elastic analysis (see, for example [3,4]). Measures of certain combinations of stresses and displacements local to the point of contact between a fretting peg and a substrate calculated from an elastic analysis have been proposed for correlating the onset of crack nucleation [5,6]. To date, the approach to life prediction using these measures has been largely empirical. However, a recent attack has been launched on the behavior of cracks emerging from the most highly stressed region at the edge of a fretting peg [7], and a preliminary study of the plasticity taking place in the contact zone has been published [8].

As a step towards the development of a mechanics of fretting damage, the present paper

* Corresponding author
E-mail address: Hutchinson@husm.harvard.edu (J.W. Hutchinson)

PII: S0013-7944(99)00002-8

focuses on the local plastic deformation accompanying fretting contact. Specifically, the paper investigates plastic deformation in substrates which have been coated with a thin, soft metal layer for the purpose of reducing their fretting susceptibility. The substrate is fretted by a circular, flat bottomed peg subject to a constant normal load and a fully reversed cyclic tangential load. The tangential load is assumed to be sufficiently large to cause the coating to undergo reversed yielding in shear in each cycle. Bulk cyclic stressing of the substrate is not considered. The role of the coating in the redistribution of the contact tractions is modeled. Two limiting boundary conditions for the peg–substrate interaction, as modified by the coating, are proposed and analyzed. Generally, plasticity in the substrate is limited to the immediate vicinity of the edge of the peg. This makes possible the formulation of a small-scale yielding problem wherein the relevant load factors become amplitudes characterizing the elastic solution at the peg corner. The approach closely parallels the small scale yielding analysis of crack tip plasticity, where the plastic zone is embedded within the elastic field whose amplitude is the stress intensity factor.

2. Asymptotic Formulations for Small Scale Yielding in Fretting

The geometry of the flat-bottom cylindrical peg in contact with the semi-infinite coated

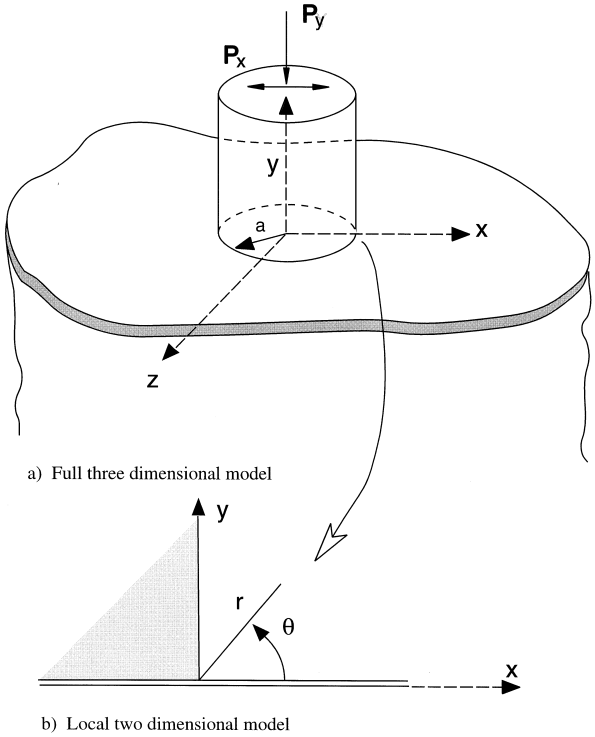

Fig. 1. (a) Three-dimensional fretting geometry. (b) Local two-dimensional geometry at right corner of fretting peg.

substrate is shown in Fig. 1. The radius of the peg, a, is assumed to be very large compared to the coating thickness. The ratio of the shear yield stress of the thin film coating, τ_y^{f}, to that of the substrate, τ_y^{s}, is one of the important parameters in the model. The metals comprising the coating and the substrate are each taken to be elastic–perfectly plastic and characterized by von Mises yield surfaces. The Young's modulus and Poisson's ratio of the substrate are E and ν (Poisson's ratio is taken to be 0.3 for all the calculations reported here). A constant downward vertical force P_Y is exerted by the peg on the substrate. The peg is displaced back and forth tangential to the substrate under nonslip conditions. The amplitude of the tangential cyclic displacement is assumed to be large enough such that the shear stress of the coating is reached everywhere under the peg (i.e. the peak tangential force attains $P_X = \pm\pi a^2 \tau_y^{\mathrm{f}}$ in each cycle). This assumption reflects the function of the soft coating and controls the maximum stresses exerted by the peg on the substrate, as will be detailed subsequently.

For realistic levels of loading, plastic deformation in the substrate is confined to a small annulus about the rim of the peg. The maximum extent of the cyclic plastic zone from the rim will be found to be less than several percent of the radius of the peg radius a. The smallness of the zone permits a small scale yielding formulation to be developed where the plastic zone is embedded within the elastic field local to the edge. Thus, to analyze and present results for plastic behavior, one need not consider the full geometry in Fig. 1. Instead, one can focus on portions of the edge of most concern and introduce amplitude factors characterizing the local elastic fields. The approach closely parallels that employed extensively and effectively in the small-scale yielding approach to crack tip plasticity. In the present study, attention is focused on the leading (and, by symmetry, trailing) edge of the peg in the vicinity of ($X = a$, $Y = 0$, $Z = 0$) in Fig. 1a. The coordinate system local to the edge of interest is defined in Fig. 1b.

The choice of boundary conditions to model the interaction of the peg and the coated substrate is not straightforward. Two sets of boundary conditions are introduced here which are expected to bracket the range of cyclic plastic behavior at the leading edge of the peg. The first set is termed the *uniform normal traction formulation*, and the second will be referred to as the *uniform normal displacement formulation*. In each, the tangential traction exerted on the substrate at the peak of the cycle is the shear yield stress in the coating. The two sets are taken in turn with discussion of the elastic amplitude factors and associated near-edge fields used to characterize the respective small scale yielding problems.

2.1. The uniform normal traction formulation

As remarked above, the cyclic tangential displacement of the peg relative to the substrate is assumed to be sufficiently large such that at the peak of the cycle in either direction the coating is yielded in shear at all points under the peg. Thus at the peak of the cycle the magnitude of the shear stress σ_{XY} acting on the substrate in the region $X^2 + Z^2 \le a^2$ is τ_y^{f}. A second implication which follows from the fact that the thin coating beneath the peg is at yield in shear is that the coating can only support an additional hydrostatic pressure p. The nonzero components of stress in the coating at the loading peak are

$$\sigma_{ij} = -p\delta_{ij} \quad \text{with} \quad \sigma_{XY} = \pm\tau_y^{\mathrm{f}} \tag{1}$$

An elementary application of equilibrium of the coating reveals that p must be independent of X and Y beneath the peg. The pressure beneath the peg becomes uniform when the elastic–perfectly plastic coating is fully yielded in shear. This argument ignores a small region at the edge of the peg on the order of the coating thickness, consistent with the underlying assumption that the film thickness is very small compared to all other length scales of interest. Thus, Eq. (1) implies that the tractions acting on the surface of the substrate in the region $X^2+Z^2\le a^2$ at the peak of the cycle are

$$\sigma_{YY} = -P_Y/\pi a^2$$

$$\sigma_{XY} = P_X/\pi a^2$$

$$\sigma_{YZ} = 0 \quad \text{with} \quad P_X = \pm \pi a^2 \tau_y^{\mathrm{f}} \tag{2}$$

where the sign of the shear traction depends on the direction of the peg displacement.

The construction of the elastic solution for a half-space subject to Eq. (2) is well known. It makes use of solutions for concentrated loads acting on the surface of the half-space [9,10]. Integral representations for the stresses can be obtained by a straightforward superposition of the concentrated load solutions over the circular portion of the surface, $X^2+Z^2\le a^2$. The stresses at any point in the substrate off the edge of the circle can be evaluated with high accuracy using numerical integration techniques widely available in numerical analysis software packages. The stresses at the edge of the peg are logarithmically singular at the edge of the peg in the elastic solution. Specifically, in the plane $Z=0$ in the vicinity of the leading edge (Fig. 1b), the local stress distribution is

$$\sigma_{xx} = \frac{P_X}{\pi a^2}\left\{\frac{2}{\pi}\ln\left(\frac{r}{a}\right) + \frac{1}{\pi}(\sin\theta)^2 + c_{xx}\right\} + \frac{P_Y}{\pi a^2}\left\{\frac{1}{\pi}\theta + \frac{1}{2\pi}\sin 2\theta + c_{xy}\right\}$$

$$\sigma_{yy} = \frac{P_X}{\pi a^2}\left\{-\frac{1}{\pi}(\sin\theta)^2\right\} + \frac{P_Y}{\pi a^2}\left\{\frac{1}{\pi}\theta - \frac{1}{2\pi}\sin 2\theta\right\}$$

$$\sigma_{zz} = \frac{P_X}{\pi a^2}\left\{\frac{2\nu}{\pi}\ln\left(\frac{r}{a}\right) + \nu c_{xx} + c_{zx}\right\} + \frac{P_Y}{\pi a^2}\left\{\frac{2\nu}{\pi}\theta + \nu c_{xy} + c_{zy}\right\}$$

$$\sigma_{xy} = \frac{P_X}{\pi a^2}\left\{-\frac{1}{\pi}\theta - \frac{1}{2\pi}\sin 2\theta\right\} + \frac{P_Y}{\pi a^2}\left\{\frac{1}{\pi}(\sin\theta)^2\right\} \tag{3}$$

Note that for the convention used here, positive P_Y acts downward. This representation of the stresses near the leading edge of the peg contains both the logarithmically singular contributions and all contributions which do not vanish as r approaches zero. The local field is a state of generalized plane strain because the strain component ε_{zz} is bounded but nonzero at $r=0$:

$$\varepsilon_{zz} = \frac{1}{\pi a^2 E}\{P_x c_{zx} + P_y c_{zy}\} \tag{4a}$$

The four coefficients in Eq. (3) have been obtained numerically such that Eq. (3) reproduces the full three-dimensional solution as r approaches zero:

$$c_{xx} = -0.190$$

$$c_{xy} = -0.165$$

$$c_{zx} = -0.220$$

$$c_{zy} = 0.190 \tag{4b}$$

The domain of accuracy of the asymptotic distribution Eq. (3), has been checked by a comparison with numerical results for the full three-dimensional solution. Comparisons indicate that the field Eq. (3), provides a good approximation (e.g. better than 5% accuracy) in the plane $Z=0$ for $r \leq a/10$.

In small scale yielding, the plastic zone must be sufficiently small compared to the peg radius a such that the stress field in an annular region outside the zone is accurately given by Eq. (3). Effectively, this means the plastic zone must be small compared to $a/10$. The concept is very similar to that used in crack tip plasticity studies. In the numerical approach used in the next section, the distribution, Eq. (3), is used to generate tractions on a circular boundary 'remote' from the origin at $r=0$.

2.2. The uniform normal displacement formulation

The formulation just described relies on the soft metal coating to redistribute the normal traction beneath the peg such that it becomes uniform at the peak of the cycle when the coating yields in shear. This process requires that the coating be thick enough to flow and redistribute the normal traction. Redistribution would be somewhat thwarted by strain hardening in the coating, the more so the thinner the coating. An alternative formulation of the substrate loading is proposed which ignores the tendency of the coating to redistribute the normal traction, while continuing to account for yielding of the coating in shear. A uniform displacement u_Y, together with a uniform shear traction $\sigma_{XY} = \pm\tau^{\mathrm{f}}_{y}$, is imposed on the substrate over the circular region under the peg. The displacement u_Y is chosen such that the average normal compressive stress under the peg is $\bar{\sigma} = P_Y/\pi a^2$. This formulation is consistent with a rigid peg and no normal traction redistribution by the coating. It is expected to overestimate the stresses in the vicinity of the peg edge.

The two-dimensional plane strain version of this alternative formulation is studied in this paper. The elastic version of this problem has uniform displacement u_y and uniform shear traction, $\sigma_{xy} \equiv \tau = \pm\tau^{\mathrm{f}}_{Y}$, prescribed on the surface for $|x| \leq [a$ and zero tractions for $|x| \geq a$, where the uniform displacement is chosen such that under the peg the average normal compressive stress is $\bar{\sigma}$. The elastic solution to this problem can be obtained using complex function methods. The stresses in the vicinity of the peg edge (i.e. near the origin in Fig. 1b) are

$$\sigma_{xx} = \frac{\bar{\sigma}}{2\pi}\sqrt{\frac{a}{2r}}\left\{3\sin\frac{\theta}{2} + \sin\frac{5\theta}{2}\right\} + \frac{\bar{\tau}}{2}\left\{\frac{1}{\pi}\left[4\ln\frac{r}{2a} - \cos 2\theta + 1\right] - \frac{1}{2}\left(\frac{\kappa-1}{\kappa+1}\right)\sqrt{\frac{a}{2r}}\left[3\sin\frac{\theta}{2} + \sin\frac{5\theta}{2}\right]\right\}$$

$$\sigma_{yy} = \frac{\bar{\sigma}}{2\pi}\sqrt{\frac{a}{2r}}\left\{5\sin\frac{\theta}{2} - \sin\frac{5\theta}{2}\right\} + \frac{\bar{\tau}}{2}\left\{\frac{1}{\pi}[\cos 2\theta - 1] - \frac{1}{2}\left(\frac{\kappa-1}{\kappa+1}\right)\sqrt{\frac{a}{2r}}\left[5\sin\frac{\theta}{2} - \sin\frac{5\theta}{2}\right]\right\}$$

$$\sigma_{xy} = \frac{\bar{\sigma}}{2\pi}\sqrt{\frac{a}{2r}}\left\{\cos\frac{\theta}{2} - \cos\frac{5\theta}{2}\right\} - \frac{\bar{\tau}}{2}\left\{\frac{1}{\pi}[\sin 2\theta + 2\theta] + \frac{1}{2}\left(\frac{\kappa-1}{\kappa+1}\right)\sqrt{\frac{a}{2r}}\left[\cos\frac{\theta}{2} - \cos\frac{5\theta}{2}\right]\right\} \tag{5}$$

with $\sigma_{zz} = \nu(\sigma_{xx} + \sigma_{yy})$ and where $\kappa = 3 - 4\nu$ in plane strain. Once again, the sign convention is such that positive $\bar{\sigma}$ implies an average compressive stress acting downward. The elastic solution has an inverse square root singularity in the stresses, in addition to the weaker logarithmic singularity produced by the tangential shear load $\bar{\tau}$. The contribution associated with the normal load $\bar{\sigma}$ is identical to the mode I distribution at the tip of a plane strain crack. An additional mode I contribution is induced by the shear load $\bar{\tau}$, due to the fact that the surface under the peg is constrained against rotation. The domain of accuracy of Eq. (5) relative to the full plane strain solution is similar to that discussed for the other formulation.

2.3. Numerical model

Finite element formulations of the two small scale yielding problems have been used to generate behavior in the plastic zone in the substrate under cyclic fretting loads. The two primary dimensionless system parameters are: (i) the ratio of the steady normal load to the cyclic shear load; and (ii) the ratio of the coating yield stress to that of the substrate. Tractions consistent with either Eqs. (3) or (5) are applied on a circular boundary remote from (and centered on) the origin $r = 0$ in Fig. 1b. The choice of remote boundary is arbitrary as long as it is sufficiently large compared to the plastic zone; $r = a/5$ was used. As remarked at the beginning of this section, the materials comprising the coating and the substrate are each taken to be elastic–perfectly plastic with von Mises yield surfaces. The behavior of the coating is incorporated through the tractions applied to the surface of the substrate directly under the pin.

The boundary conditions were imposed by prescribing nodal forces or displacements that are consistent with either Eq. (3) or Eq. (5). Displacement fields associated with the asymptotic stress fields in Eqs. (3) and (5) were derived. For the outer radius, the choice of whether to prescribe tractions or displacements is somewhat arbitrary, but prescribing displacements is

generally favored as they did not involve elemental integration to determine nodal forces. Under the pin, the constant shear traction boundary condition was imposed by prescribing nodal forces in the x-direction which resulted in a constant shear stress. For the uniform normal pressure case, nodal forces in the vertical direction were used consistent with this loading. The generalized plane strain cases involved the additional requirement of specifying the strain in the direction normal to the plane of the model according to the prescription (4a).

The finite element solutions were generated using the commercial code ABAQUS with eight-noded quadrilateral plane strain elements. (Generalized plane strain elements were used for the case of uniform normal tractions by specifying the out-of-plane strain component.) It is assumed that behavior closer to the origin than about $r = a/100$ from the model need not be resolved, both because the fidelity of the model becomes questionable (e.g. the finite thickness of the coating is not taken into account) and because the length scale relevant to fatigue crack nucleation will usually be larger than this. The mesh consisted of 1000 elements in a radial fan focusing on the origin. Results from a coarser mesh with approximately 1000 elements in a radial fan focusing on the origin. Results from a coarser mesh with approximately 600 elements revealed negligible differences in plastic strain values outside $r = a/100$. Since run times were not significantly different for the two meshes, the finer mesh was used for all the calculations.

A cycle is defined as going from maximum shear load in one direction to an equivalent

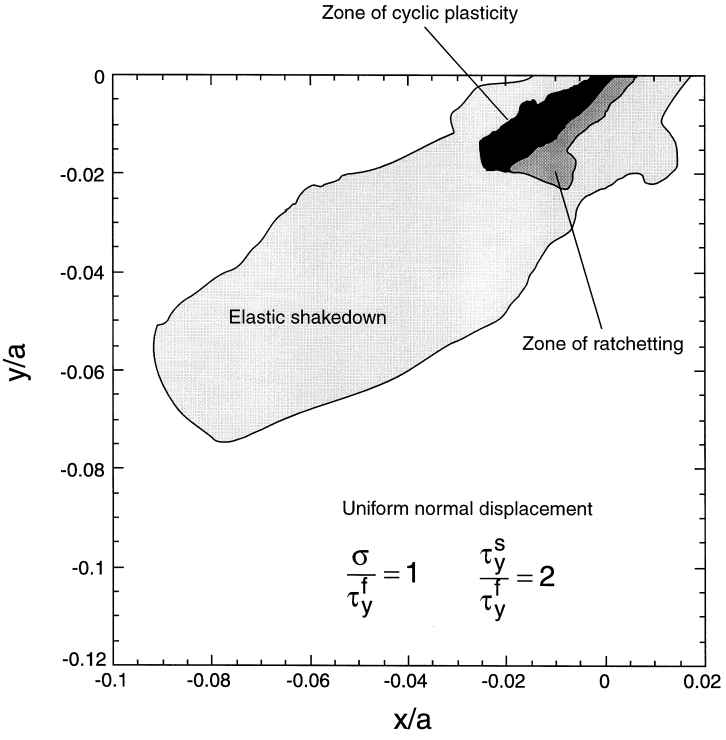

Fig. 2. Plastic zones in the vicinity of the right corner of the peg for the formulation of uniform normal displacement.

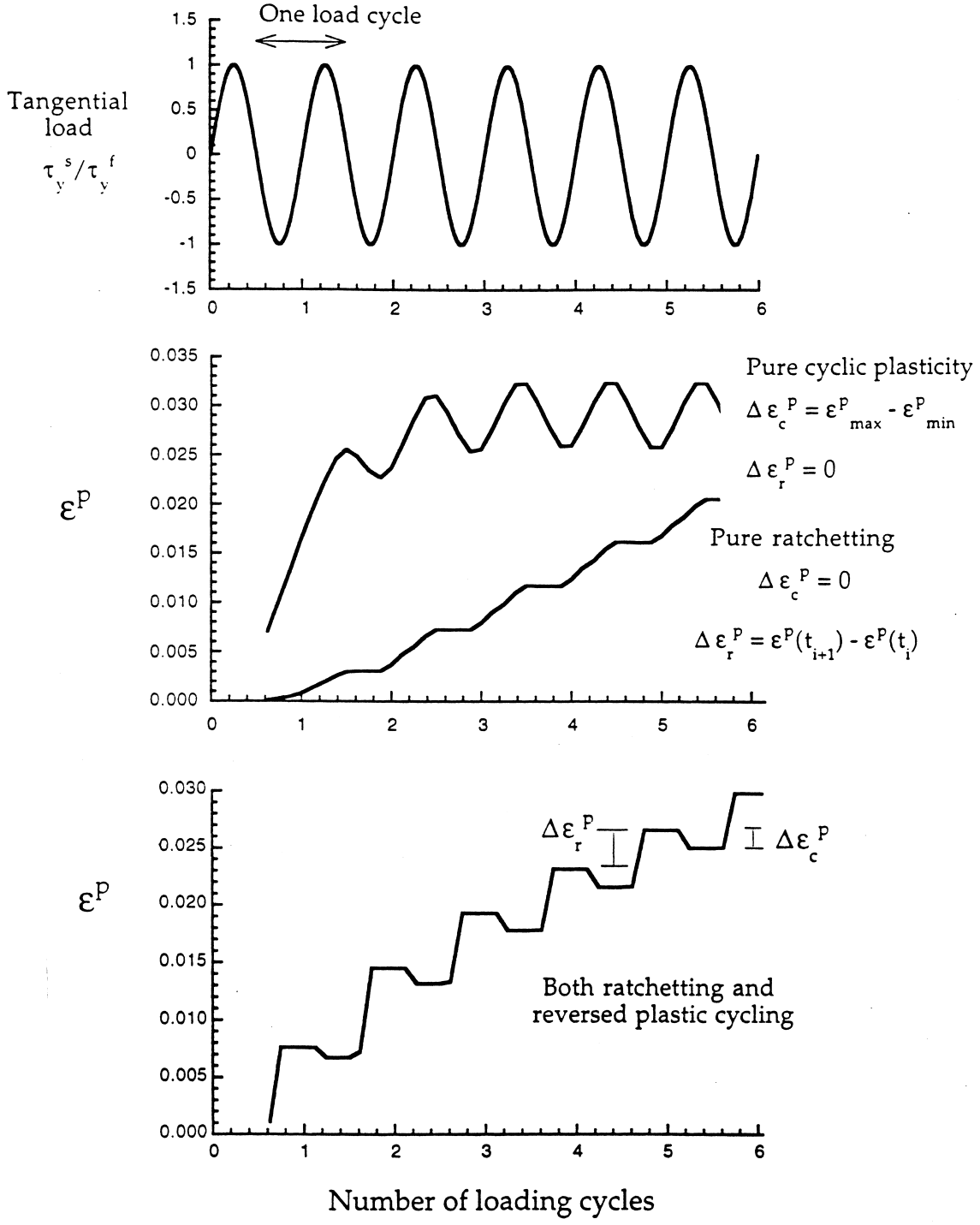

Fig. 3. Schematic of the different types of cyclic plastic strain responses.

magnitude in the opposite direction, and returning again to the first maximum shear load. By this definition, a quarter cycle is needed to increase the applied loads from zero to the first maximum. Both shear and normal loads were first increased from zero to their maximum values in direct proportion; then, the normal load was held fixed, while the tangential load was cycled. Six full cycles were simulated after the loads were brought to their initial maxima. Care was taken to ensure that the imposed boundary conditions (displacements or nodal forces) properly account for the cyclic component from the shear traction and the constant component from the normal displacement or pressure. This is achieved by computing the individual contributions from each type of loading and superimposing them at each time in the cycle.

3. Plasticity in the substrate

Behavior in the plastic zone is fairly complex. To aid the discussion, a detailed plastic zone map is given in Fig. 2 for a specific set of parameters. The example is for the uniform normal displacement formulation, but details for the other formulation are qualitatively similar. The outer boundary, extending out to just over $a/20$ from the peg edge, is the zone of plastic deformation occurring in the first loading cycle when the normal load is brought up to its maximum value along with the shear load. From the peak of the first cycle, the normal load is held constant and the shear load is cycled. The outer portion of the initial plastic zone experiences no further plastic strain increments after the first or second cycle. (At some points, no further plastic increments occur after the time corresponding to maximum negative shear.) The outer portion of the zone experiences elastic shakedown. Plastic strain increments continue to occur in subsequent cycles in the inner portion of the plastic zone, extending to a distance of approximately $0.03a$ from the origin for this example. The zone of active incremental plasticity can be divided into two sub-zones, one dominated by ratchetting behavior and the other by cyclic plastic strains. Precise definitions of these terms within the present context will now be given.

3.1. Elastic shakedown, cyclic plastic straining and ratchetting

Four types of response at points within the initial plastic zone are indicated in Fig. 3 for a representative component of plastic strain, ε^{p}. At the top of the figure, the cyclic tangential loading history is indicated with integer values of time coinciding with the beginning of one cycle and the end of the one before. The initial load application in which the normal load is brought up to its constant maximum occurs between $t=0$ and $1/4$. In the portion of the initial plastic zone where elastic shakedown occurs, elastic unloading occurs following the peak of the first or second cycle and the yield condition is never again reached. To distinguish between cyclic plastic staining and ratchetting, consider first pure limits of these behaviors shown in Fig. 3. In pure cyclic straining each plastic strain component oscillates between minimum and maximum values which do not change after the first few cycles. Repeatable reversed plasticity occurs with yielding necessarily taking place under both positive and negative shearing of the peg. Such behavior has been termed ‘plastic shakedown’ by some authors. Pure ratchetting involves an increment of the plastic strain component in each cycle associated with shearing in

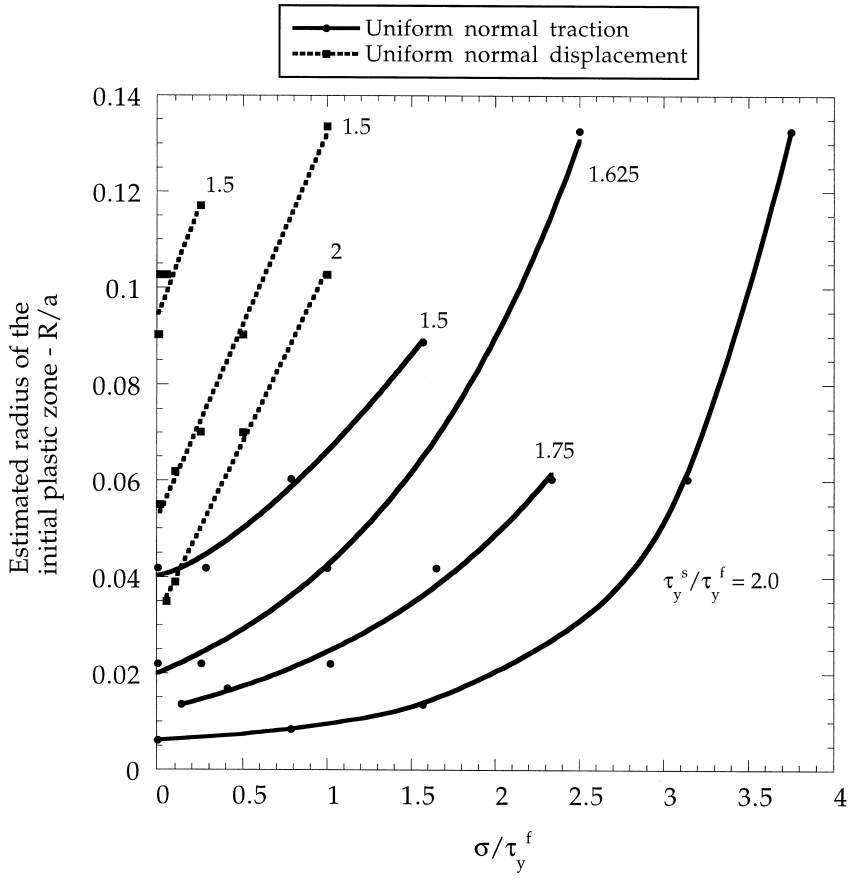

Fig. 4. Size of the plastic zone at the peak of the first load cycle as dependent on the two dimensionless system parameters, σ/τ^{f}_{y} and $\tau^{s}_{y}/\tau^{f}_{y}$, and the model formulation.

one direction but not the other. Reversed plastic straining does not occur. The increment per cycle, $\Delta\varepsilon^{p}_{r}$, is constant after the first few cycles. Generally, neither pure cyclic plastic straining nor pure ratchetting occur in the fretting problem, although this behavior may occur at localized regions in the plastic zone. At a typical point within the zone of active plasticity a combination of these two responses are observed to take place, as depicted in the bottom sketch in Fig. 3. Here again, after the first one or two cycles, the behavior settles down to a repeatable pattern in which a fixed amplitude of reversed cyclic plastic straining, $\Delta\varepsilon^{p}_{c}$, occurs simultaneously with a fixed amplitude of ratchetting, $\Delta\varepsilon^{p}_{r}$. The two sub-zones referred to in connection with Fig. 2 are defined consistent with which class of deformation is dominant. Further definitions needed to ascertain the cyclic and ratchetting amplitudes in terms of all the component of strain are given below.

For the case depicted at the bottom of Fig. 3 involving combined cyclic plasticity and ratchetting, define the plastic ratchetting strain once the deformation has settled down as the difference in plastic strains at any two comparable times in the loading history (such as the points of maximum tangential shear) of two subsequent cycles according to:

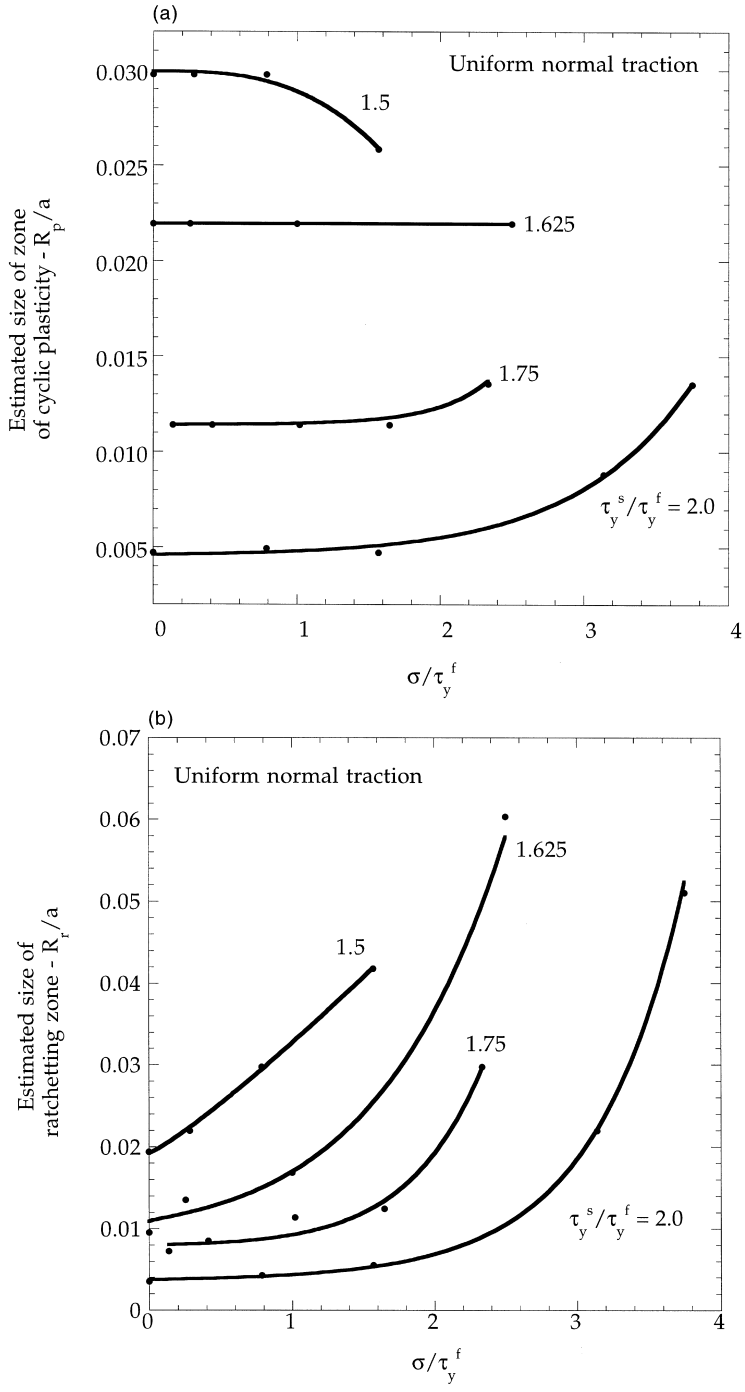

Fig. 5. Size of the active plastic zones for the uniform normal traction model. (a) Zone of cyclic plasticity. (b) Zone of ratchetting plasticity.

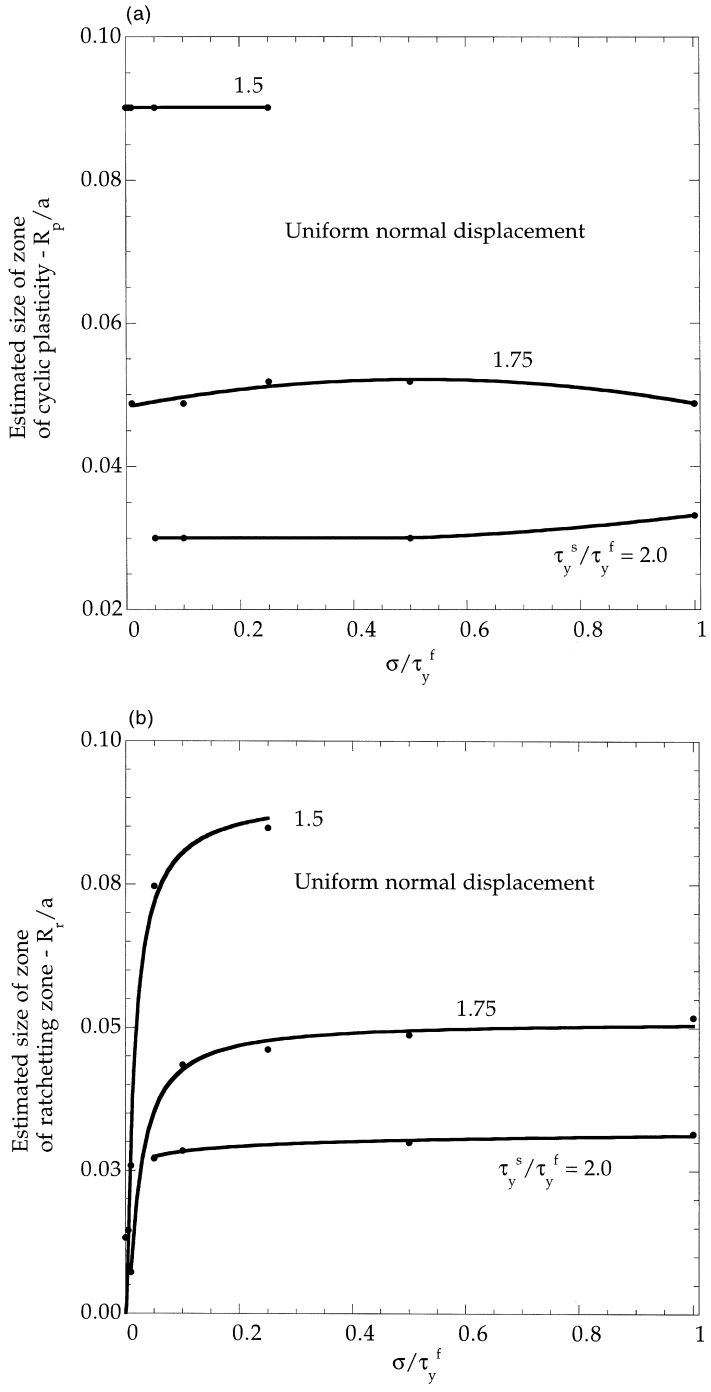

Fig. 6. Size of the active plastic zones for the uniform normal displacement model. (a) Zone of cyclic plasticity. (b) Zone of ratchetting plasticity.

$$(\Delta\varepsilon_{ij}^{p})_{r} = \varepsilon_{ij}^{p}(t_{i+1}) - \varepsilon_{ij}^{p}(t_i) \tag{6}$$

The cyclic plastic strain can then be defined as (see Fig. 3):

$$(\Delta\varepsilon_{ij}^{p})_{c} = (\varepsilon_{ij}^{p})_{max} - (\varepsilon_{ij}^{p})_{min} - (\Delta\varepsilon_{ij}^{p})_{r} \tag{7}$$

where the first two values represent the maximum and minimum values of the components in a given cycle. These values are almost always attained at points where the shear load undergoes reversal in direction. Effective measures of the amplitudes are used. The effective cyclic plastic strain is defined as[1]

$$\Delta\varepsilon_{c}^{p} = \sqrt{\tfrac{2}{3}(\Delta\varepsilon_{ij}^{p})_{c}(\Delta\varepsilon_{ij}^{p})_{c}} \tag{8}$$

and the ratchetting strain amplitude is

$$\Delta\varepsilon_{r}^{p} = \sqrt{\tfrac{2}{3}(\Delta\varepsilon_{ij}^{p})_{r}(\Delta\varepsilon_{ij}^{p})_{r}} \tag{9}$$

With reference to the sub-zones in Fig. 2, the zone of cyclic plastic straining has $\Delta\varepsilon_{c}^{p} > \Delta\varepsilon_{r}^{p}$, while the ratchetting zone has $\Delta\varepsilon_{r}^{p} > \Delta\varepsilon_{c}^{p}$.

3.2. Size of initial plastic zone and zones of cyclic plasticity and ratchetting

It is already evident from Fig. 2 that a soft coating cannot fully isolate the substrate from plastic deformation. The size of the initial plastic zone at the end of the first full load cycle when the normal load attains its maximum value is shown in Fig. 4 as a function of the two primary parameters, $\tau_{y}^{s}/\tau_{y}^{f}$ and σ/τ_{y}^{f} where σ is the average normal compressive stress exerted by the peg. After the first cycle, subsequent loading does not change the size of the plastic zone. The zone associated with the uniform normal displacement conditions is substantially larger than that associated with uniform normal traction. Otherwise, the trends are in accord with intuition: the initial zone size increases with harder coatings and with larger normal peg force.

The roles of $\tau_{y}^{s}/\tau_{y}^{f}$ and σ/τ_{y}^{f} in determining the size of the zones of cyclic plasticity and ratchetting are shown in Figs. 5 and 6. The size of the zone of cyclic plastic straining is specified by the requirement that $\Delta\varepsilon_{c}^{p}$ must be greater than 1% of the uniaxial strain at yield ($\varepsilon_{y} = \sqrt{3}\tau_{y}/E$).[2] Analogous requirements are made on the effective ratchetting strains in the definition of the ratchetting zone. Ratchetting generally occurs at locations dominated by cyclic plastic straining, and vice versa. As such, the delineation between zones of ratchetting and cyclic plasticity is qualitative.

The average normal compressive traction σ has little influence on the size of the zone of cyclic plastic straining for either of the two sets of boundary conditions. On the other hand, the yield stress ratio, $\tau_{y}^{s}/\tau_{y}^{f}$, has a strong effect on the zone size. Decreasing the flow stress of

[1] The summation convention is implied for all repeated indices.

[2] The additional requirement that $\Delta\varepsilon_{c}^{p}$ must be larger than $\Delta\varepsilon_{r}^{p}$ does not significantly alter the figures; this additional requirement was used to delineate between ratchetting and cyclic plasticity 'zones' in Fig. 2.

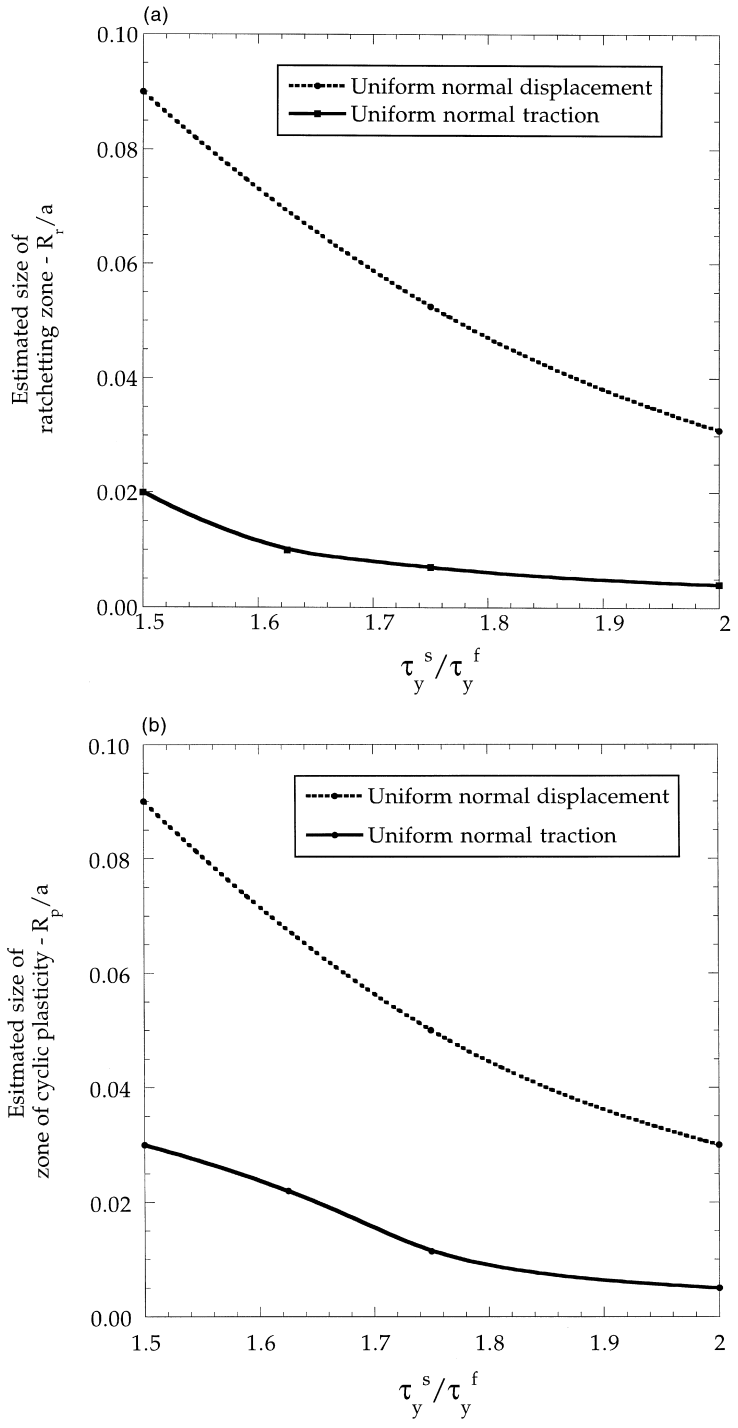

Fig. 7. Approximate size of the active plastic zones as a function of τ_y^s/τ_y^f. The results for most of the range for which σ/τ_y^f does not exceed unity. (a) Zone of cyclic plasticity. (b) Zone of ratchetting plasticity.

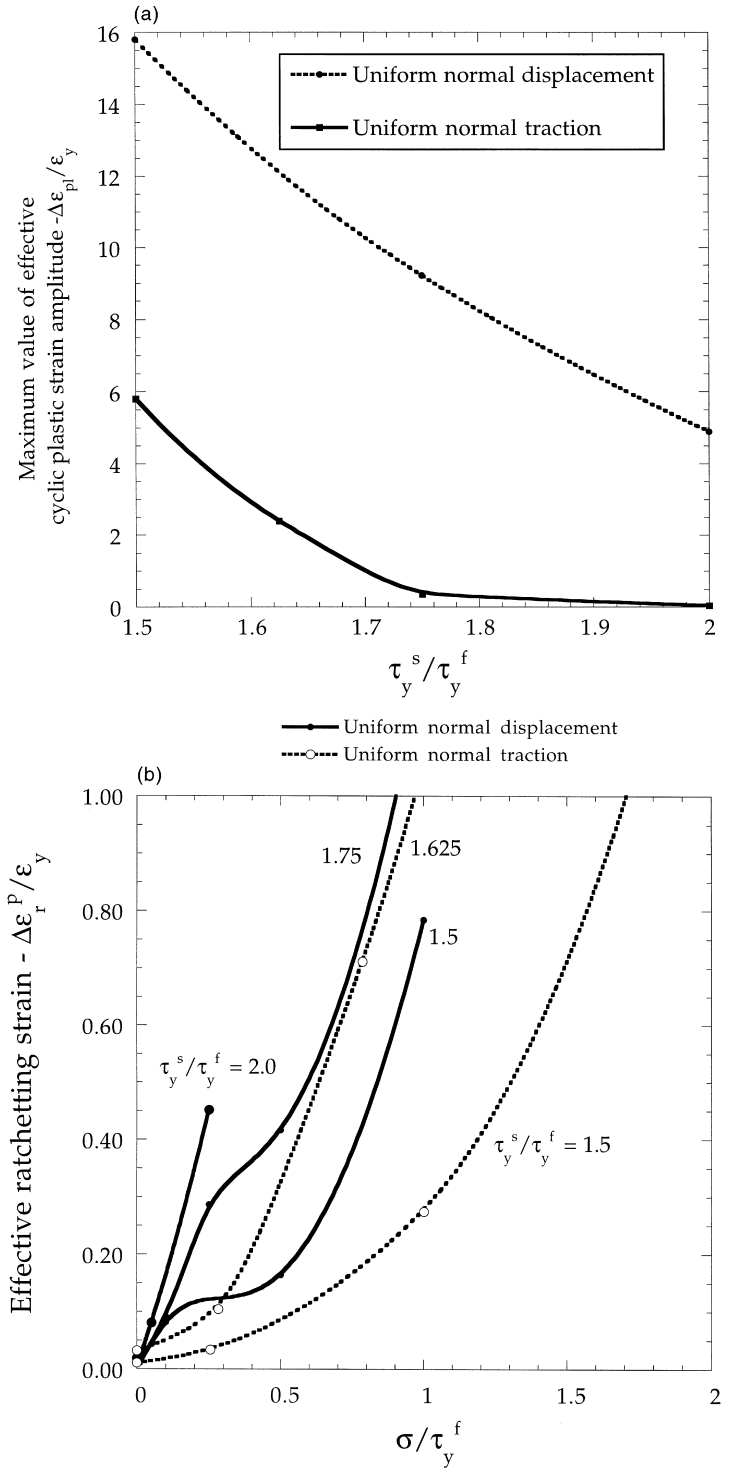

Fig. 8. Maximum value of the effective plastic strain amplitudes occurring each cycle outside the circle $r/a=0.01$ centered at the peg corner ($\sigma/\tau_y^f=1$). (a) Maximum cyclic plastic strain amplitude (for all values of σ/τ_y^f considered). (b) Ratchetting strain amplitudes as a function of normal loading.

the coating from 2/3 to 1/2 of the flow stress of the substrate results in a dramatic reduction in the size of both the zone of cyclic plastic straining and the ratchetting zone. The average normal traction has a fairly large effect on the ratchetting zone size, especially for the case of uniform normal tractions. At low σ/τ_y^f the cyclic plastic zone is larger than the ratchetting zone, but the ratchetting zone becomes the larger of the two as the normal pressure from the peg increases.

The same results are presented in a different manner in Fig. 7, where the estimated size of the respective zones are shown as a function of τ_y^s/τ_y^f. The size of the zone of cyclic plastic straining has been plotted using data in the range where it is relatively independent of σ/τ_y^f. Only at the highest values of σ/τ_y^f do the lower curves in Fig. 7a, b significantly underestimate the zone size for the uniform normal traction model. The upper curves in Fig. 7a, b, which apply to the uniform normal displacement model, have been plotted using values at the high end of the range of σ/τ_y^f, and thus these curves represent the upper limit for this model.

The two sets of results taken together should bound the zone sizes, because the uniform normal traction model undoubtedly exaggerates the ability of the coating to redistribute the normal traction near the peg corner while the uniform normal displacement model almost certainly underestimates the effect. The trends of Fig. 7 further emphasize the important role played by the coating hardness in determining the size of the cyclic and ratchetting plastic zones in the substrate.

3.3. Plastic strains

The trends in plastic zone size are complemented by the curves of Fig. 8 showing the maximum of the effective cyclic plastic strain outside the circle $r/a=0.01$ surrounding the peg corner as a function of the yield stress ratio. Here, $\Delta\varepsilon_e^p$ is the amplitude of the effective cyclic plastic strain, where any ratchetting contribution has been removed via Eq. (7). As suggested by the fact the cyclic plastic zone size is insensitive to the average normal traction (Figs. 5a and 6a), the magnitude of the effective cyclic plastic strain is insensitive as well. Indeed, increasing the average normal traction will generally *decrease* the maximum of the effective cyclic plastic strain; as such the curves in Fig. 8 represent upper bounds on the cyclic plastic strain. The amplitude decreases strongly with decreasing coating flow stress. The uniform normal traction model predicts the cyclic plastic strain amplitude falls to almost zero for $r/a>0.01$ if $\tau_y^s/\tau_y^f \geq 1.75$. By contrast, the other model indicates that significant cyclic plastic straining will still occur, although the amplitude decreases sharply with increasing τ_y^s/τ_y^f.

The magnitude of the effective ratchetting strain amplitude has a much stronger dependence on the average normal traction and increases sharply with increasing normal loading. This phenomena is illustrated in Fig. 8b. As such, it is impossible to place upper bounds on the magnitude of ratchetting strain amplitude for a given τ_y^s/τ_y^f, as was done in Fig. 8a. It is interesting to note that for the uniform normal displacement case, the ratchetting strain amplitude will increase significantly with increasing normal pressure, despite the fact that the ratchetting zone *size* does not increase (see Fig. 6b). For all uniform normal displacement cases, the effective ratchetting amplitude is an order of magnitude smaller than the effective cyclic plastic strain. For the uniform normal traction cases where $\tau_y^s/\tau_y^f > 1.6$, the ratchetting strain amplitudes are comparable with effective cyclic plastic strains.

The two plastic sub-zones extend under the peg at roughly a 135–150° angle to the surface (Fig. 2). At higher values of the normal pressure in the uniform normal traction case, there is an additional 'lobe' of the plastic zone which extends at roughly 60° (at a right angle to the primary plastic zone). Ratchetting zones dominate this portion of the plastic zone. The deformation in the cyclic zone comprises significant reversed plastic shearing parallel to the zone. Plastic straining in the ratchetting zone is consistent with material being squeezed out from under the peg emerging at the surface just to the right of the peg corner. Ratchetting is

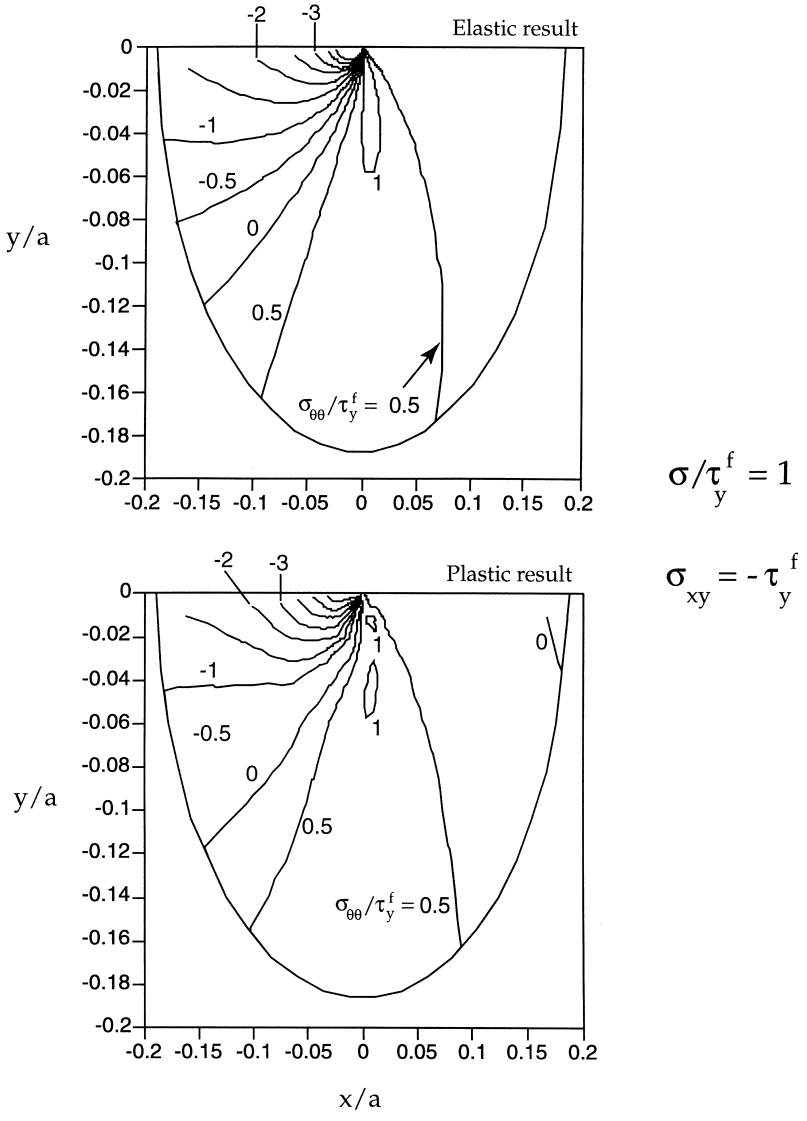

Fig. 9. Contours of constant values of $\sigma_{\theta\theta}/\tau_y^f$ near the peg corner at the point in the loading cycle when $\sigma_{xy} = -\tau_y^f$ for the uniform normal displacement formulation with $\sigma/\tau_y^f = 1$ and $\tau_y^s/\tau_y^f = 2$. The horizontal and vertical axes are x/a and y/a.

expected to cause a redistribution of normal traction under the corner of the indenter. The local traction distribution will vary slowly from cycle to cycle as material is squeezed out from the immediate vicinity of the corner. It is not evident how this process saturates.

Fig. 9 displays the distribution of the circumferential component of stress, $\sigma_{\theta\theta}$, at every point in the vicinity of the peg corner in the sixth cycle at the point where the peg is at the peak negative tangential displacement (i.e. $\sigma_{xy} = -\tau_y^f$ under the peg). These distributions are for the uniform normal displacement model with system parameters identical to those for the plastic zones in Fig. 2. A plot for the corresponding elastic solution is also shown in Fig. 9, indicating there is no significant qualitative difference between the two fields and, in particular, in the predicted regions of tensile hoop stress. Tensile circumferential stresses occur in a fan of approximately 40° centered on $\theta \cong -80°$ under the peg corner. The combination of active plastic straining and tensile stress is expected to promote the formation of fatigue cracks. Note that the tensile stresses at the right corner of the peg only occur during the portion of the cycle when the shearing force exerted by the peg is directed to the left.

4. Summary of findings and implications for fretting

The zones of cyclic and ratchetting plasticity in the substrate extend beneath the peg at an angle of approximately 35° to the peg–substrate interface ($\theta = -145°$). It is suggestive that the plastic zones (as depicted in Fig. 2) are aligned with the direction of crack nucleation in experiments (e.g. [1,11,12]). The size of these active plastic zones diminish sharply with softer substrate coatings (i.e. with diminishing τ_y^f/τ_y^s). As long as the integrity of a soft coating is preserved, it is highly effective at lowering stresses in the most highly stressed region under a fretting peg. Tensile circumferential stresses occur below the peg during the portion of the cycle when the peg is sheared away from the respective corner. These stresses are also lowered by lowering the coating yield stress. The zone of active plasticity and the region experiencing tensile circumferential stress overlap only in a small region at the peg corner, but their proximity suggests that the substrate is likely to be susceptible to fatigue cracks emerging from the corner downward at an angle somewhere in the range $-135° < \theta < -45°$. The direction of the emerging fatigue crack at the corner of a peg fretting an uncoated substrate has been studied using an elastic analysis in [4].

The role of ratchetting strains in fretting failure is not clearly understood, probably due in large part to the fact that predictive approaches have been based almost exclusively on elastic analyses (a typical approach is to use elastic effective strain amplitudes in a Coffin–Manson relationship [1]). However, there has been some work done to investigate the role of ratchetting strains on cyclic failure [13,14]. Johnson suggests two modes of failure: low cycle fatigue (LCF) (dominated by cyclic plastic strains) and ratchetting fatigue (RF) (dominated by ratchetting strains). Johnson and Kapoor summarize experimental evidence that supports the notion that the number of cycles to failure will show a different dependence on cyclic strain amplitude and ratchetting strain amplitude.

In other words, different Coffin–Manson relationships would be needed for LCF and RF, and failure will be governed by whichever predicts a shorter lifetime [13]. In this context, the implication of the results presented here is that increasing the average normal traction may

switch failure mechanisms from LCF to RF, and significantly alter the crack nucleation time scale. Furthermore, the transition point from LCF to RF would depend on the ratio τ_y^f/τ_y^s. As far as ratchetting failure is concerned, it remains to be resolved whether increasing τ_y^f/τ_y^s would have as strong an effect of lifetimes as implied in Fig. 8a and b. It would depend strongly on the magnitude of the average normal traction, unlike failure governed by cyclic plasticity.

The quantitative difference between the predictions from the two asymptotic formulations, uniform normal tractions and uniform normal displacements, is appreciable. The uniform normal displacements formulation predicts significantly more plasticity activity than the other formulation. Further modeling will be required before it is clear which of the two formulations is the more accurate. It is expected that the thickness of the coating will play a role in determining the plasticity activity in the substrate, as will any tendency of the coating to display cyclic strain hardening or softening.

Acknowledgements

The authors are indebted to helpful discussions with A. G. Evans and to D. N. Hutchinson who carried out the comparisons of the asymptotic elastic stress fields with the full three-dimensional elastic fields. This work is supported in part by the Multi-University Research Initiative on 'High Cycle Fatigue', which is funded at Harvard by AFSOR under grant no. SA1542-22500 PG, and in part by the Division of Engineering and Applied Sciences, Harvard University.

References

[1] Waterhouse RB. Fretting fatigue. Int Mater Rev 1992;37:77–97.
[2] Cowles BA. High cycle fatigue in aircraft gas turbines—an industrial perspective. Int J Fracture 1996;80:147–63.
[3] Helmi Attia M, Waterhouse RB, editors. Standardization of fretting fatigue test methods and equipment STP 1159. Philadelphia, PA: ASTM.
[4] Hills DA, Nowell D. Mechanics of fretting fatigue. Dordrecht: Kluwer Academic, 1994.
[5] Ruiz C, Boddington PHB, Chen KC. An investigation of fatigue and fretting in a dovetail joint. Exp Mech 1984;24:208–17.
[6] Szolwinski MP, Farris TN. Mechanics of fretting fatigue crack initiation. Wear 1996;198:193–207.
[7] Giannakopoulos AE, Lindley TC, Suresh S. Aspects of equivalence between contact mechanics and fretting mechanics: theoretical connections and life prediction methodology for fretting fatigue. Acta Materialia (in press).
[8] Giannakopoulos AE, Suresh S. A three-dimensional analysis of fretting fatigue. Acta Materialia 1997;46:177–92.
[9] Timoshenko SP, Goodier JN. Theory of elasticity, 3rd ed. New York: McGraw-Hill, 1970.
[10] Johnson KL. Contact mechanics. Cambridge: Cambridge University Press, 1985.
[11] Anton DL, Guillemette R, Reynolds J, Lutian M. Fretting fatigue damage analysis in Ti-6Al-4 V. In: Gregory JK, Rack HJ, Eylon D, editors. Surface performance of titanium. The Mineral, Metals and Materials Society, 1997.
[12] Sato K, Fujii H, Kodama S. Crack propagation behavior in fretting fatigue. Wear 1986;107:245–62.
[13] Johnson KL. Contact mechanics and the wear of metals. Wear 1995;190:162–70.

[14] Kapoor A. A re-evaluation of the life to rupture of ductile materials by cyclic plastic strain. Fatigue Fract Engng Mater Struct 1994;17:201–19.